Journal of the Meteorological Society of Japan

EARLY ONLINE RELEASE

The DOI for this manuscript is

DOI:10.2151/jmsj.2021-034

J-STAGE Advance published date: February 22nd, 2021

Investigating Runoff Sensitivity in the Land-Surface Model MATSIRO to Reduce Low Runoff Bias

Kumiko TAKATA [1,2]

[1]*National Institute for Environmental Studies, Ibaraki, Japan*
[2]*Azabu University, Kanagawa, Japan*

and

Naota HANASAKI

National Institute for Environmental Studies, Ibaraki, Japan

First submission to J. Meteor. Soc. Japan on April 26, 2020
Revised submission to J. Meteor. Soc. Japan on July 31, 2020
Second-revised submission to J. Meteor. Soc. Japan on December 28, 2020

----

1) Corresponding author: Kumiko Takata, Azabu University, 1-17-71, Fuchinobe, Chuo-ku, Sagamihara-shi, Kanagawa 252-5201 JAPAN.
Email: k-takata@azabu-u.ac.jp
Tel: +81-42-754-1111(ex.2589)

Abstract

The Minimal Advanced Treatments of Surface Interaction and RunOff (MATSIRO), which has been used as a land-surface scheme in the global climate model, the Model for Interdisciplinary Research On Climate (MIROC), calculates Dunne runoff and base runoff using the TOPography-based MODEL (TOPMODEL). In past experiments that used MATSIRO, the runoff and its response to precipitation were too low compared to observation. We conjectured that those biases could be attributed to the water table's excessive depth. Its depth was diagnosed based on grid-mean soil moisture, using a saturation threshold that was originally set to almost equal the porosity. In this study, sensitivity experiments, in which the threshold was decreased to 75%, 50%, 25%, and less than 13% of the porosity, were conducted, and the subsequent effects on river flow were investigated in the Chao Phraya River basin, Thailand, as a case study. As a result, both Dunne and base runoff increased along with the response of river flow to precipitation. The simulated river flow matched observations most closely with the threshold of 50% saturation. In addition, soil moisture and the Bowen ratio also changed significantly with the runoff changes induced by the threshold changes. These results suggested the importance of the relationship between grid-mean soil moisture and groundwater level for TOPMODEL. Preliminary global experiments indicate that the runoff sensitivity might be dependent on climate zone.

Keywords land-surface model; runoff; soil saturation; water table depth; Chao Phraya River basin

1. Introduction

The importance of the role of terrestrial hydrological processes in climate change has been widely recognized since the 1980s (Manabe and Wetherald, 1987), and the effects of vegetation canopy have also been incorporated (Sellers *et al*., 1996). The Minimal Advanced Treatments of Surface Interaction and RunOff (MATSIRO; Takata *et al*., 2003; Nitta *et al*., 2014) model represents land-surface processes in a global climate model, the Model for Interdisciplinary Research on Climate (MIROC; e.g., Tatebe *et al*., 2019). MIROC is a core model used for climate change projections in the Intergovernmental Panel on Climate Change (IPCC) assessment reports, and MATSIRO has been used in various comparisons of land-surface hydrological models (e.g., Veldkamp *et al*., 2017).

In land-surface models used for climate studies, such as MATSIRO, spatiotemporal distributions of surface temperature, evapotranspiration, runoff, soil moisture and temperature, snow cover, and other variables are calculated from energy and water balances at the ground surface. In the past, MATSIRO significantly underestimated runoff compared to observations. A parameter for base runoff was calibrated (Hirabayashi *et al*., 2005), and the algorithm for diagnosing the depth of the groundwater table was improved (Yoshimura *et al*., 2006) at a global scale. Yet, MATSIRO still belongs to a group of land-surface models with low runoff (e.g., Fig. 2a of Haddeland *et al*., 2011).

In this study, we investigated the behavior of MATSIRO, focusing specifically on the runoff generation mechanism (i.e., the relationship between the water table depth and soil moisture). We conducted offline experiments using meteorological data for the Chao Phraya River basin in Thailand as a case study to see whether daily runoff values can be close to observation.

2. Method

2.1 Study area

We performed a numerical experiment for the Chao Phraya River basin in Thailand, for which high-resolution input and verification data are available. The average annual temperature in Thailand from 1981 to 2010 was 26.9°C; the annual precipitation was 1,588 mm, with 1,265 mm during the rainy season (May to October) and 322 mm during the dry season (November to April; Thai Meteorological Department, 2015). The Chao Phraya River basin has an area of approximately 160,000 km^2 and extends from central Thailand to the northern part of the country. The northern part of the basin is mountainous (with an altitude of about 1,500 m), and the central and southern parts are made up of vast plains (Fig.1). There are two major dams: the Bhumibol dam, on the Ping River in the western upstream area, and the Sirikit dam, on the Nan River in the eastern upstream area. These dams are responsible for controlling floods in the rainy season and supplying water for irrigation in the dry season (Shintani *et al*., 1994). The Bhumibol dam was selected for analysis in this study; it has a catchment area of 26,214 km^2 and a total water storage capacity of approximately 13,462 MCM (GRanD v1.1, http://globaldamwatch.org/grand/).

Fig. 1

2.2 Model

MATSIRO was developed as a model of land-surface hydrological processes for a global climate model. It calculates surface temperature and heat and moisture fluxes using energy and water balances at the ground surface. The following processes are taken into consideration: the effects of the vegetation canopy on radiation, interception of precipitation, turbulent fluxes, and transpiration (modeled with a single layer), the accumulation and ablation of snow (with a variable number of model layers between one and three), and the moisture and temperature conduction in soil. Soil is divided into six layers with depths of 0–5 cm, 5–25 cm, 25–100 cm, 1–2 m, 2–4m, and 4–14 m, from the surface to the bottom. See Takata *et al*. (2003) and Nitta *et al*. (2014) for details.

The four types of runoff considered in our calculations are overland runoff when the soil moisture in the uppermost layer exceeds the porosity, infiltration excess runoff (known as Horton runoff) when the precipitation intensity exceeds the infiltration capacity at the ground surface, saturation excess runoff (known as Dunne outflow) which is generated from the runoff contributing area or saturated zone, and base runoff (Fig. 2). The sum of these four types of runoff is taken as the total runoff at each grid point. Dunne and base runoff are calculated based on the TOPography-based MODEL (TOPMODEL; Beven and Kirkby, 1979; Sivapalan *et al*., 1987; Stieglitz *et al*., 1997) by simplifying the subgrid-scale topography in a grid box.

Dunne runoff is generated from the runoff contributing area, taken as the saturated zone, calculated using the TOPMODEL. In addition, overland runoff and infiltration excess runoff (Horton runoff) are considered to be generated outside the contributing area. Fig. 2

Dunne runoff, Q_{dunne}, is calculated by multiplying precipitation by the contributing area (A_s), and A_s is calculated from the water table depth (z_{WTD}) on the basis of TOPMODEL using the following equation:

$$Q_{dunne} = A_s \times P, \qquad \text{Eq.(1)}$$

where

$$A_s = 1 - \exp(f \times z_{WTD} - 1), \qquad \text{Eq.(2)}$$

P is the precipitation intensity at the ground surface, and f is the vertical attenuation parameter of permeability set uniformly to 3.0 (unit: m^{-1}). z_{WTD} (unit: m) is downward positive; a large positive value means a deep water-table depth. A_s is set to 0 when it is shown to be negative based on Eq.(2); namely, z_{WTD} is deeper than one third meter. The relationship between A_s and z_{WTD}, Eq.(2), is deduced from the analytical solution of the quasi-stationary condition of recharge and base flow in TOPMODEL. z_{WTD} is diagnosed from soil moisture using a procedure explained below.

The base runoff (Q_{base}) is also calculated based on TOPMODEL, as follows:

$$Q_{base} = K_0 \exp(1 - f \times z_{WTD}) \tan(\beta) / (f \times L), \qquad \text{Eq.(3)}$$

where K_0 is the surface permeability specified according to soil type, and β and L are subgrid topographic parameters for the slope angle and length defined based on the standard deviation of altitude within a grid cell.

z_{WTD} is diagnosed using two steps. In the first step, the grid-mean matric potential (unit: m) in the k-th soil layer (numbered from the surface) is examined to assess whether water table can exist in it. If water table is expected to be in the k-th layer, in the second step, saturation judgment is conducted with the grid-mean volumetric soil moisture content in the k-th layer (θ_k, unit: m^3 m^{-3}) as follows:

"Saturated": $\theta_k > \theta_s - \varepsilon_{GW}$, Eq.(4a)

"Unsaturated": $\theta_k < \theta_s - \varepsilon_{GW}$, Eq.(4b)

where θ_s is the porosity, the saturation value (i.e., maximum) of θ_k, ranging from 0.404 to 0.465 specified according to soil type; ε_{GW} is a threshold of saturation judgment in diagnosing z_{WTD}, a standard value being 0.001. When it is judged to be "unsaturated," the existence and the depth of water table (z_{WTD}) are diagnosed in the layer. When it is judged to be "saturated," the water table is assumed as being in a shallower layer, and the above two steps are conducted in the adjacent upper layer ($k - 1$). The procedure begins at the bottom layer and is repeated for the upper layers until it is judged to be "unsaturated." In short, z_{WTD} is diagnosed as being within the deepest "unsaturated" layer. Since the standard value of ε_{GW} is small, it is diagnosed as "unsaturated" when θ_k is slightly below θ_s. Consequently, z_{WTD} tends to be deep in MATSIRO. When z_{WTD} is diagnosed as being deeper than the bottom of the deepest layer, Q_{base} and A_s are considered to be zero.

The total runoff, which is the sum of all runoff components calculated at each grid point, flows down along the river channel network scheme, the Total Runoff Integrating Pathways

(Oki and Sud, 1998). In this study, the spatial resolution of the channel network is 5 arcmin (modified from Kotsuki and Tanaka, 2013), and a constant flow velocity (0.3 m s^{-1}) is assumed.

2.3 Experiments and analyses

We used the surface atmospheric data from the Integrated study on Hydro-Meteorological Prediction and Adaptation to Climate Change in Thailand (IMPAC-T) Forcing Dataset (IFD-K10) of Kotsuki *et al*. (2014). This dataset includes precipitation, pressure and wind speed at a temporal resolution of 1 h, temperature and downward longwave radiation at a temporal resolution of 3 h, and humidity and downward shortwave radiation at a daily temporal resolution. Precipitation, which is one of the most important climate variables for runoff simulation, was derived from the gauge-based daily data in combination with the satellite-based mean monthly diurnal variation. The precipitation was thus rather representative as actual precipitation on a daily or longer time scale since it was based on gauged data (Kotsuki and Tanaka, 2013), though its diurnal changes could include uncertainty. The time step of the model was set to 60 minutes. When the time of the input data and the time of the model simulation do not match, time interpolation is performed using the before-and-after input data, except that the daily shortwave radiation was divided into an hourly value accounting for the solar zenith angle. The study area was bounded by the coordinates 97–102°E and 13–20°N, with a spatial resolution of 5 arcmin (approximately 9 km) for the period 1981–2004. The initial condition was taken by conducting a separate spin-up experiment with recursive forcing of 1981, and it was used for all the sensitivity experiments. In our analyses, we used results for 1993 and 2002 as case studies of low- and high-precipitation years, respectively. Vegetation distribution and monthly averaged leaf area index in 2000 (Takata and Hanasaki, 2020) were used.

In the control experiment (denoted EP.0), ε_{GW} was set to the standard value of 0.001; in our sensitivity experiments EP.1, EP.2, EP.3, and EP.4, this value was changed to 0.1, 0.2, 0.3, and 0.4, respectively (Table 1). Considering that θ_s ranged from 0.404 to 0.465 depending on soil type, a soil layer was judged to be "saturated" when θ_k was more than approximately 0.3, 0.2, 0.1, and 0.004–0.06 in EP.1, EP.2, EP.3, and EP.4, respectively (Eq. 4). In other words, it was judged to be "saturated" when θ_k was approximately 75%, 50%, 25%, and only 1–13% of the porosity in the sensitivity experiments. Consequently, z_{WTD} is expected to become shallow if the vertical profile of soil moisture is the same because z_{WTD} is diagnosed as being within the deepest "unsaturated" layer (see section 2.2). The saturation area (A_s) is then expected to increase (Eq. 2); Q_{dunne} (Eq. 1) and Q_{base} (Eq. 3) are also expected to increase (Eq. 3). Note that the soil moisture calculation remained unchanged in this study. Only the threshold (ε_{GW}) for saturation judgment in diagnosing z_{WTD} was changed in examinations of the runoff sensitivity.

Table 1

We compared the observed river flow at the Bhumibol dam inlet to the calculated river flow at the model grid point nearest to the Bhumibol dam and examined the sensitivity to ε_{GW}. In addition, the sensitivity of runoff, z_{WTD}, and soil moisture to ε_{GW} were investigated in the catchment area of the Bhumibol Dam. Modeled river flow was compared directly to observations because there is no large reservoir or irrigation water intake upstream of the dam, and the river flow scheme in MATSIRO does not consider such human operations.

In addition, the sensible heat flux, the latent heat flux, and the Bowen ratio (i.e., the ratio of sensible heat fluxes to latent heat fluxes) was compared with the observation to examine the effects of the sensitivity experiments on surface energy and water balances. The observation data from Kim *et al*. (2014) recorded at Tak (16°56.390′N, 99°25.793′E; located about 50 km downstream of the Bhumibol dam) using the eddy correlation method were provided. The data were compared with the calculated results at the grid point nearest to Tak.

3. Results

Fig. 3 shows the time series of daily rainfall (used as model input values) averaged over the catchment of the Bhumibol dam and the time series of daily river flow at the inlet of the dam. The results from a low-precipitation year (1993, 724 mm year^{-1}) and a high-precipitation year (2002, 1221 mm year^{-1}) are shown; mean precipitation during the study period (1981-2004) was 968 mm year^{-1}. For both years, the control experiment EP.0 showed that river flow was significantly underestimated compared to observations, and there was almost no response of river flow to precipitation. The Nash–Sutcliffe efficiency (*NSE*), one of the most widely used validation indices for hydrology models, was calculated to compare

Fig. 3

the modeled daily river flow with the observation as follows:

$$NSE = 1 - \Sigma_t(Q_m(t) - Q_o(t))^2 \,/\, \Sigma_t(Q_o(t) - Q_{o\,mean})^2, \qquad \text{Eq.(5)}$$

where $Q_m(t)$ is the modeled daily river flow at time t, $Q_o(t)$ is the observed daily river flow at time t, $Q_{o\,mean}$ is the mean observed daily river flow during the analysis period, and Σ_t denotes the sum during the analysis period. NSE ranges from negative infinity to 1.0, with NSE = 1 being the optimal value (Moriasi *et al.*, 2007). The NSEs in EP.0 were −0.357 and −0.376, respectively, in 2002 and 1993 (Table 2); values lower than 0.0 are generally regarded as unacceptable. River flow increased slightly in EP.1 but was similar to EP.0 in both years. In EP.2, EP.3, and EP.4, river flow increased, and the response to precipitation increased markedly for 2002. The results of EP.2 were closest to the observations and showed a smoothed response to precipitation (at approximately a 10-day scale). NSE in 2002 was 0.250, generally regarded as acceptable though unsatisfactory; NSE in 1993 was 0.763, generally regarded as good (Moriasi et al., 2007). In EP.3, modeled river flow was greater than the observations in the rainy season. Furthermore, in EP.4, river flow was also greater than the observations in the dry season. The peaks in the modeled river flow occurred later in all sensitivity experiments than they had in the observations. The changes in river flow with respect to ε_{GW} were similar in both years.

Fig. 4 shows the time series in 2002 of the modeled z_{WTD}, Q_{dunne}, and Q_{base} averaged over the Bhumibol dam catchment area for the control and sensitivity experiments. The results in the high-precipitation year are shown since seasonal changes are generally marked in high- Fig. 4

precipitation years. Note that the arrival of peaks for Q_{dunne} and Q_{base} were earlier than those of river flow at the inlet of the dam because of the time for passing through the river channels. In EP.0 and EP.1, z_{WTD} showed similar seasonal change throughout the year; it deepened gradually from January to May, reaching a maximum depth of about 6 m, subsequently rose, and became shallowest at about 5 m in December. z_{WTD} in EP.2 was much shallower; it deepened from January to May, became deepest at about 3 m, subsequently rose, and became shallowest at about 0.5 m in early September, followed by a gradual deepening to December. Some smoothed increases occurred in response to precipitation events in November at intra-monthly time scales. In EP.3 and EP.4, z_{WTD} was even shallower and did not deepen from January to May, remaining at a depth of 1.8 m in EP.3 and 1 m in EP.4. Quick rises in response to precipitation (at a time scale of approximately 5 days) were more marked than seasonal changes.

The groundwater level measured from July to December in 2006 at the Kog Ma D site in the Bhumibol dam catchment area (Shiraki *et al.*, 2017) rose from July to early September; the shallowest depth was approximately 1.5 m. It deepened toward December, reaching about 2 m deep. Although it is not possible to make a direct comparison owing to the difference between the observation and experimental periods and the difference in the spatial scales, the seasonal change of z_{WTD} in EP.2 qualitatively agreed with the observation; it showed a gradual rise until early September followed by gradual deepening until December.

Q_{dunne} and Q_{base} both increased with increasing ε_{GW}. Q_{dunne} markedly increased between EP.1 and EP.2 and between EP.2 and EP.3, which suggests that sensitivity of Q_{dunne} was great near ε_{GW} = 0.2 (as in EP.2). Q_{base} hardly changed between EP.0 and EP.1 but increased significantly in EP.2, EP.3, and EP.4. In EP.2, Q_{base} increased gradually from the beginning of the rainy season (from May), peaking in September, with responses to precipitation until November. In EP.3, Q_{base} increased in May, subsequently decreased in June and July, then increased again with a peak in September with marked responses to precipitation during the rainy season. By contrast, in EP.4, Q_{base} increased in May and remained high throughout the rainy season.

Our results show that as the saturation threshold ε_{GW} increased, z_{WTD} became shallower, Q_{dunne} and Q_{base} became larger, and river flow increased. The increase in Q_{dunne} was led by the increase in the saturated zone A_s, which induced decreases in infiltration of precipitation Fig. 5
into the soil, reducing soil moisture. Fig. 5 shows the vertical profiles of monthly soil moisture, averaged over the catchment of the Bhumibol dam in 2002 for the experiments EP.0, EP.2, and EP.4. In EP.0, A_s was small and infiltration into soil was large. Thus, soil moisture was high and its seasonal amplitude at the surface was large, reaching to the fifth layer (2–4 m) (Fig. 5a). Since ε_{GW} was 0.001 for EP.0, the bottom layer (4-14 m) was the deepest "unsaturated" layer and the water table averaged over the catchment was diagnosed as varying between 4.8–5.9 m deep in 2002 (Fig. 4a). In EP.2 (ε_{GW} = 0.2), A_s became larger and infiltration into the soil decreased. Consequently, soil moisture and its seasonal

amplitude tended to be lower and smaller than EP.0 (Fig. 5b). The deepest "unsaturated" layer varied from the third to the fifth layers (0.25–4 m), and the water table averaged over the catchment was diagnosed as varying between 0.5–3.1 m deep in 2002. In EP.4, A_s was much larger, infiltration was much smaller, and soil moisture and its amplitude were much smaller (Fig. 5c); the water table averaged over the catchment was much shallower (varying between 0.1–1.1 m in 2002; Fig. 4a).

Such changes in soil moisture influence not only runoff (i.e., water balance at the surface) but also energy balance at the surface. In examining the effects of the sensitivity experiments on the surface energy and water balance, the sensible heat fluxes, the latent heat fluxes and the Bowen ratios were examined along with comparison to observation at Tak. Fig. 6 shows the monthly values in 2003 and 2004, when the periods of observation and numerical experiments overlapped. The both fluxes and the Bowen ratios showed seasonal changes similar to the observations. The latent heat fluxes were overall smaller than the observations, though, because of the difference in spatial scale and meteorological conditions between the experiments and the observations. The values of the both fluxes and the Bowen ratios for EP.0 and EP.1 were almost the same and their seasonal amplitudes were smaller than the observations. The seasonal amplitudes of the both fluxes became large for EP.2; the amplitude of the Bowen ratio was as large as the observations. In EP.3 and EP.4, the seasonal amplitudes of the Bowen ratio were larger than the observations, because of the high sensible heat fluxes and the low latent heat fluxes particularly in the dry

Fig. 6

seasons. These results imply that the change in ε_{GW} has significant effects not only on runoff but also on the energy and water balance at the ground surface.

4. Discussion

4.1 Implications based on sensitivity

MATSIRO is a land-surface hydrology scheme used in the global climate model MIROC, a major model used by the IPCC to make global warming projections since the fourth assessment report (Randall *et al*., 2007). Although the capability of MIROC is rated highly because of, for example, its ability to reproduce an El Niño event (Watanabe *et al*., 2010), runoff in MATSIRO has been underestimated in various offline experiments at global and regional scales (e.g., Haddeland *et al*., 2011). The method used in this study's sensitivity experiments is extremely simple but has not been tried since the model was developed, and it markedly changed runoff in the study area. We speculate that this is because of the conceptual gaps between the assumptions of TOPMODEL and the application in MATSIRO.

Specifically, TOPMODEL calculates Q_{dunne} from the contributing area according to topographical structure and Q_{base} from groundwater with quasi-stationary recharge on slopes in small watersheds. In MATSIRO, these concepts are applied to a grid point whose size ranges from a regional scale (e.g., 10 km) to a global scale (e.g., 100 km). Thus, treatment of subgrid heterogeneity in topography and water table depth is essential to apply the TOPMODEL concept to a relatively large grid cell such as MATSIRO. The threshold change in this study is believed to exemplify such treatment.

The seasonal changes in river flow, which increased from the latter half of August to October, agreed with the observation in EP.2 (Fig. 3). However, the peaks in response to the intra-seasonal peaks of precipitation in September and November 2002 were approximately 10 days later than those observed. Moreover, the observed small peaks in May in response to precipitation were not represented in either year. Considering that the delays of the observed peaks from precipitation were very small, investigations into the river channel scheme and the uncertainty of observation would also be needed, but other runoff components and parameters should be further examined to sophisticate representation of the runoff response to precipitation.

Subgrid topography parameters and the vertical attenuation parameter for hydraulic conductivity can also affect runoff. In addition, the assumption of the uniform topographic index would be a tentative treatment. Lastly, possible introduction of other types of runoff should be considered including subsurface stormflow, macropores, and other preferential flow paths (Brutseart, 2005). A more realistic form of the function should be used in future land-surface models. It should also be noted that runoff sensitivity also depends on the model's temporal and spatial resolution.

4.2 Regionality of runoff sensitivity

Runoff depends on climate, geology, topography, soil characteristics, vegetation, and land use, and the predominant runoff process varies in time and space depending on the precipitation intensity and ground-surface conditions preceding precipitation (Sivapalan *et al.*, 1987). Runoff sensitivity may therefore vary regionally.

Next, global experiments were conducted offline with global surface meteorological data (ELSE; Kim *et al.*, 2009); for experiment G-EP.0 ε_{gw} = 0.001, and for experiment G-EP.2 ε_{gw} = 0.2. The horizontal resolution was 1 × 1° (about 100 km), and the study period was 1979–2004.

The global mean annual runoff (averaged from 1995 to 2004) was 199 mm year^{-1} for G-EP.0 and 327 mm year^{-1} for G-EP.2; thus, changing ε_{gw} from 0.001 to 0.2 increased the annual runoff by 64%. Fig. 7 shows the global distribution of the rate of change in annual runoff: $(Q_{G\text{-}EP.2} - Q_{G\text{-}EP.0})/(0.5 \times Q_{G\text{-}EP.2} + 0.5 \times Q_{G\text{-}EP.0})$. The runoff sensitivity to ε_{gw} was high in regions with a savanna climate (Africa, India, Indochina Peninsula, northern Australia, and South America) and regions with a subtropical dry winter climate (east China, central North America, and Western Europe). In cold regions (north of 50°N), the runoff sensitivity to ε_{gw} was moderate. By contrast, runoff was not sensitive in regions with a semiarid climate (the Middle East, western China, and western North America) or regions with a rainforest (Indonesia). In semiarid regions, changing ε_{gw} did not change z_{WTD} significantly, whereas in regions with a rainforest, where it is sufficiently humid, changes in z_{WTD} did not noticeably change the total runoff.

Fig. 7

These results show that runoff sensitivity to ε_{gw} is not globally uniform. Therefore, it is important to fully survey modeled river flow by comparing it to observations to understand the relationship between soil moisture, z_{WTD}, runoff components, and river flow.

5. Conclusions

Aiming to reduce the low biases in runoff with MATSIRO by focusing on the runoff generation mechanism, sensitivity experiments were performed to raise the water table by changing the saturation judgment threshold ε_{GW} in diagnosing z_{WTD} (i.e., without changing the soil moisture). Specifically, the threshold was set to approximately 100% (EP.0), 75% (EP.1), 50% (EP.2), 25% (EP.3), and less than 13% (EP.4) saturation. Consequently, z_{WTD} became shallow in accordance with decreasing the judgement level of "unsaturated" soil moisture, Q_{dunne} and Q_{base} increased, river flow increased, and the response of river flow to precipitation increased in the catchment area of the Bhumibol dam in the Chao Phraya River basin. The NSE for the observations was highest in EP.2 in both the high-precipitation and low-precipitation years. Soil moisture and the Bowen ratio changed significantly in accordance with the changes in ε_{GW}. The results of global experiments imply that runoff sensitivity to ε_{GW} may vary by region.

Acknowledgments

This research was supported by the Science and Technology Research Partnership for Sustainable Development (SATREPS) program of the Japan Science and Technology Agency (JST) and the Japan International Cooperation Agency (JICA), and by the Integrated

Research Program for Advancing Climate Models (TOUGOU), Grant No. JPMXD0717935457, from the Ministry of Education, Culture, Sports, Science and Technology (MEXT), Japan. The authors thank Dr. Seita Emori for providing the draft of Fig. 2.

References

Beven K. J., and M. J. Kirkby, 1979: A physically based, variable contributing area model of basin hydrology. *Hydrol. Sci. Bull.*, **24**, 43–69.

Brutseart, W., 2005: Hydrology An Introduction, Cambridge University Press, Cambridge, UK, pp605.

Haddeland, I., D. B. Clark, W. Franssen, F. Ludwig, F. Voß, N. W. Arnell, N. Bertrand, M. Best, S. Folwell, D. Gerten, S. Gomes, S. N. Gosling, S. Hagemann, N. Hanasaki, R. Harding, J. Heinke, P. Kabat, S. Koirala S, T. Oki, J. Polcher, T. Stacke, P. Viterbo, G. P. Weedon, and P. Yeh, 2011: Multimodel Estimate of the Global Terrestrial Water Balance: Setup and First Results. *J. Hydrometeor.*, **12**, 869–884.

Hirabayashi Y., S. Kanae, I. Struthers, and T. Oki, 2005: A 100-year (1901–2000) global retrospective estimation of the terrestrial water cycle. *J. Geophys. Res.: Atmos.*, **110**, D19101.

Kim H., P. J. F. Yeh, T. Oki, S. and Kanae, 2009: Role of rivers in the seasonal variations of terrestrial water storage over global basins. *Geophys. Res. Let.*, **36**, L17402.

Kim W., D. Komori, J. Cho, S. Kanae, and T. Oki, 2014: Long-term analysis of evapotranspiration over a diverse land use area in northern Thailand. *Hydrol. Res. Let.*, **8**, 45–50.

Kotsuki S., and K. Tanaka, 2013: Uncertainties of precipitation products and their impacts on runoff estimates through hydrological land surface simulation in Southeast Asia. *Hydro. Res. Let.*, **7**, 79–84.

Kotsuki S., K. Tanaka, and S. Watanabe, 2014: Projected hydrological changes and their consistency under future climate in the Chao Phraya River Basin using multi-model and multi-scenario of CMIP5 dataset. *Hydrol. Res. Let.*, **8**, 27–32.

Manabe S., and R. T. Wetherald, 1987: Large-Scale Changes of Soil Wetness Induced by an Increase in Atmospheric Carbon Dioxide. *J. Atmos. Sci.*, **44**, 1211–1236.

Moriasi, D. N. , J. G. Arnold, M. W. Van Liew, R. L. Bingner, R. D. Harmel, and T. L. Veith, 2007: Model Evaluation Guidelines for Systematic Quantification of Accuracy in Watershed Simulations. *Transac. ASABE*, **50**, 885–900.

Nitta T., K. Yoshimura, K. Takata, R. O'ishi, T. Sueyoshi, S. Kanae, T. Oki, A. Abe-Ouchi, and G. E. Liston, 2014: Representing Variability in Subgrid Snow Cover and Snow Depth in a Global Land Model: Offline Validation. *J. Clim.*, **27**, 3318–3330.

Oki T., and Y. C. Sud, 1998: Design of Total Runoff Integrating Pathways (TRIP)—A Global River Channel Network. *Earth Interactions*, **2**, 1–36.

Randall D. A., R. A. Wood, S. Bony, R. Colman, T. Fichefet, J. Fyfe, V. Kattsov, A. Pitman, J. Shukla, J. Srinivasan, R. J. Stouffer, A. Sumi, and K. E. Taylor, 2007: *Climate Change 2007: The Physical Science Basis. Contribution of Working Group I to the Fourth Assessment Report of the Intergovernmental Panel on Climate Change,* ed S Solomon*, et al.* (Cambridge, United Kingdom and New York, NY, USA: Cambridge University Press) pp 1–74.

Sellers, P. J., D. A. Randall, G. J. Collatz, J. A. Berry, C. B. Field, D. A. Dazlich, C. Zhang, G. D. Collelo, and L. Bounoua, 1996: A Revised Land Surface Parameterization (SiB2) for Atmospheric GCMS. Part I: Model Formulation. *J. Clim.*, **9**, 676–705.

Shiraki, K., N. Tanaka, T. Chatchai, and M. Suzuki, 2017: Water budget and rainfall to runoff processes in a seasonal tropical watershed in northern Thailand. *Hydrological Research Letters*, **11**, 149–154.

Sivapalan, M., K. Beven, and E. F. Wood, 1987: On hydrologic similarity: 2. A scaled model of storm runoff production. *Water Resour. Res.*, **23**, 2266–2278.

Stieglitz, M., D. Rind, J. Famiglietti, and C. Rosenzweig, 1997: An Efficient Approach to Modeling the Topographic Control of Surface Hydrology for Regional and Global Climate Modeling. *J. Clim.*, **10**, 118–137.

Takata, K., S. Emori, and T. Watanabe, 2003: Development of the minimal advanced treatments of surface interaction and runoff. *Global Planet. Change*, **38**, 209–222.

Takata, K., and N. Hanasaki, 2020: The effects of afforestation as an adaptation option: a case study in the upper Chao Phraya River basin. *Environ. Res. Let.*, **15**, 044020.

Tatebe, H., T. Ogura, T. Nitta, Y. Komuro, K. Ogochi, T. Takemura, K. Sudo, M. Sekiguchi, M. Abe, F. Saito, M. Chikira, S. Watanabe, M. Mori, N. Hirota, Y. Kawatani, T. Mochizuki, K. Yoshimura, K. Takata, R. O'Ishi, D. Yamazaki, T. Suzuki, M. Kurogi, T. Kataoka, M. Watanabe, and M. Kimoto, 2019: Description and basic evaluation of simulated mean state, internal variability, and climate sensitivity in MIROC6. *Geosci. Model Dev.*, **12**, 2727–2765.

Thai Meteorological Department, 2015: The climate of Thailand. pp 7 (https://www.tmd.go.th/en/archive/thailand_climate.pdf).

Veldkamp, T. I. E., Y. Wada, J. C. J. H. Aerts, P. Döll, S. N. Gosling, J. Liu, Y. Masaki, T. Oki, S. Ostberg, Y. Pokhrel, Y. Satoh, H. Kim, and P. J. Ward, 2017: Water scarcity hotspots travel downstream due to human interventions in the 20th and 21st century. *Nature Commun.*, **8**, 15697.

Watanabe, M., M. Chikira, Y. Imada, and M. Kimoto, 2010: Convective Control of ENSO Simulated in MIROC. *J. Clim.*, **24**, 543–562.

Yoshimura, K., S. Miyazaki, S. Kanae, and T. Oki, 2006: Iso-MATSIRO, a land surface model that incorporates stable water isotopes. *Global Planet. Change*, **51**, 90–107.

List of Figures

Fig. 6 Monthly mean (a) sensible heat fluxes (W m^{-2}), (b) latent heat fluxes (W m^{-2}), and (c) Bowen ratios, measured (black line with dots) and modeled (all other lines; see legend) at Tak in 2003–2004.

Fig. 7 Difference in annual runoff between G-EP.0 (ε_{GW} = 0.001) and G-EP.2 (ε_{GW} = 0.2), calculated as $(Q_{G\text{-}EP.2} - Q_{G\text{-}EP.0})/(0.5\times Q_{G\text{-}EP.2} + 0.5\times Q_{G\text{-}EP.0})$. Mean values from 1995–2004 are shown. The regions where the difference between $Q_{G\text{-}EP.0}$ and $Q_{G\text{-}EP.2}$ has been smaller than 1 mm $year^{-1}$ are uncolored.

List of Tables

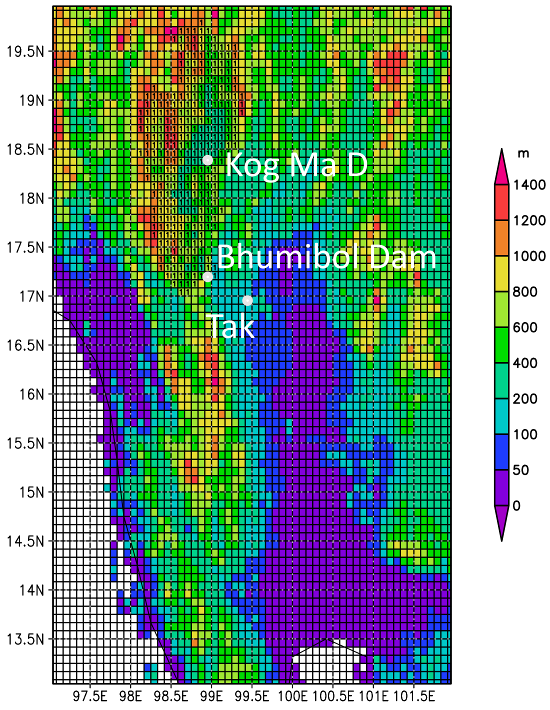
Kog Ma D
Bhumibol Dam
Tak
19.5N
19N
18.5N
18N
17.5N
17N
16.5N
16N
15.5N
15N
14.5N
14N
13.5N
97.5E
98E
98.5E
99E
99.5E
100E
100.5E
101E
101.5E
m
1400
1200
1000
800
600
400
200
100
50
0

Fig. 1

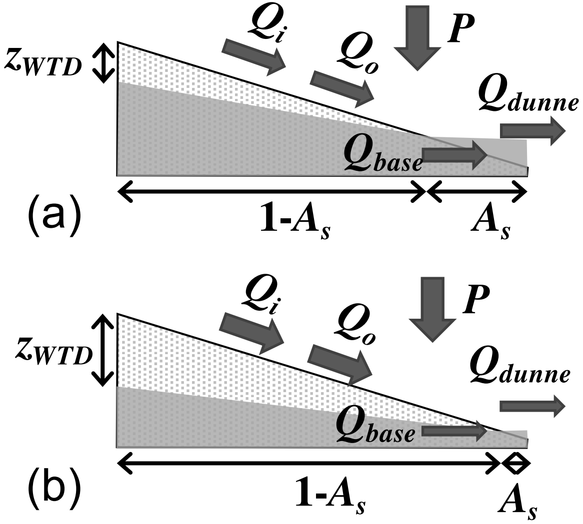

z_{WTD}
Q_i
Q_o
P
Q_{dunne}
Q_{base}
(a)
$1\text{-}A_s$
A_s
z_{WTD}
Q_i
Q_o
P
Q_{dunne}
Q_{base}
(b)
$1\text{-}A_s$
A_s

Fig. 2

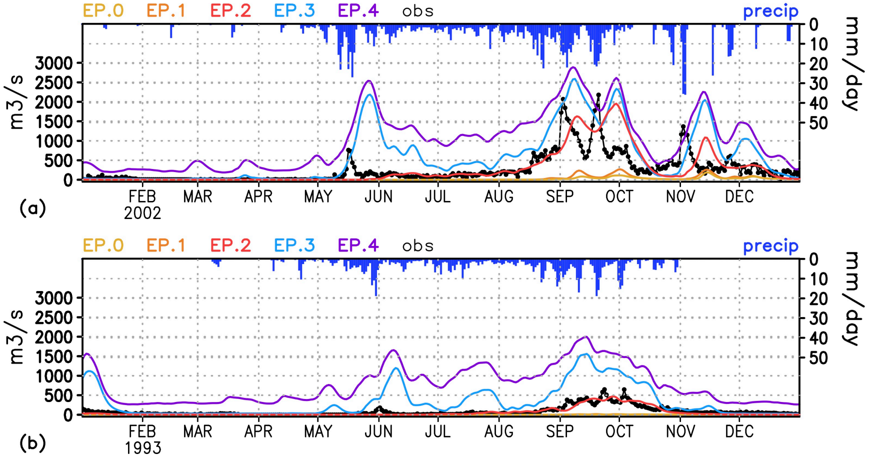
EP.0 EP.1 EP.2 EP.3 EP.4 obs
precip
m3/s
mm/day
0
500
1000
1500
2000
2500
3000
10
20
30
40
50
FEB
2002
MAR
APR
MAY
JUN
JUL
AUG
SEP
OCT
NOV
DEC
(a)
EP.0 EP.1 EP.2 EP.3 EP.4 obs
precip
m3/s
mm/day
FEB
1993
MAR
APR
MAY
JUN
JUL
AUG
SEP
OCT
NOV
DEC
(b)

Fig. 3

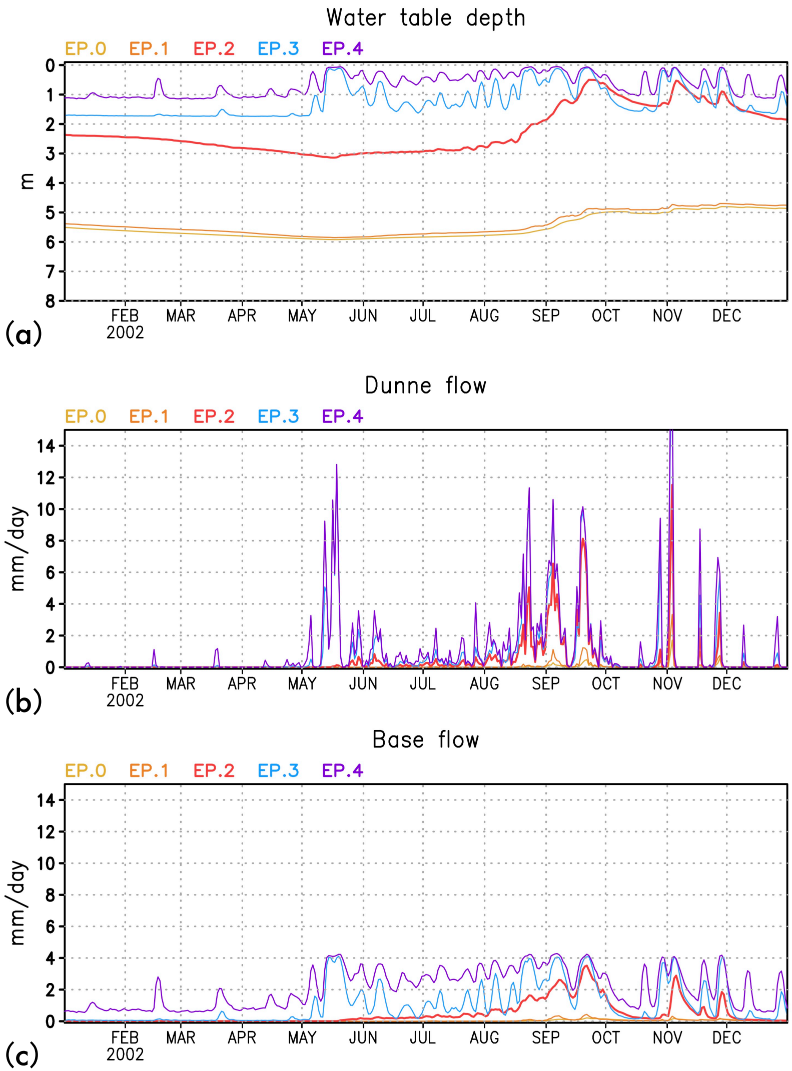
Water table depth
EP.0 EP.1 EP.2 EP.3 EP.4
m
0 1 2 3 4 5 6 7 8
FEB 2002 MAR APR MAY JUN JUL AUG SEP OCT NOV DEC
(a)
Dunne flow
EP.0 EP.1 EP.2 EP.3 EP.4
mm/day
0 2 4 6 8 10 12 14
FEB 2002 MAR APR MAY JUN JUL AUG SEP OCT NOV DEC
(b)
Base flow
EP.0 EP.1 EP.2 EP.3 EP.4
mm/day
0 2 4 6 8 10 12 14
FEB 2002 MAR APR MAY JUN JUL AUG SEP OCT NOV DEC
(c)

Fig. 4

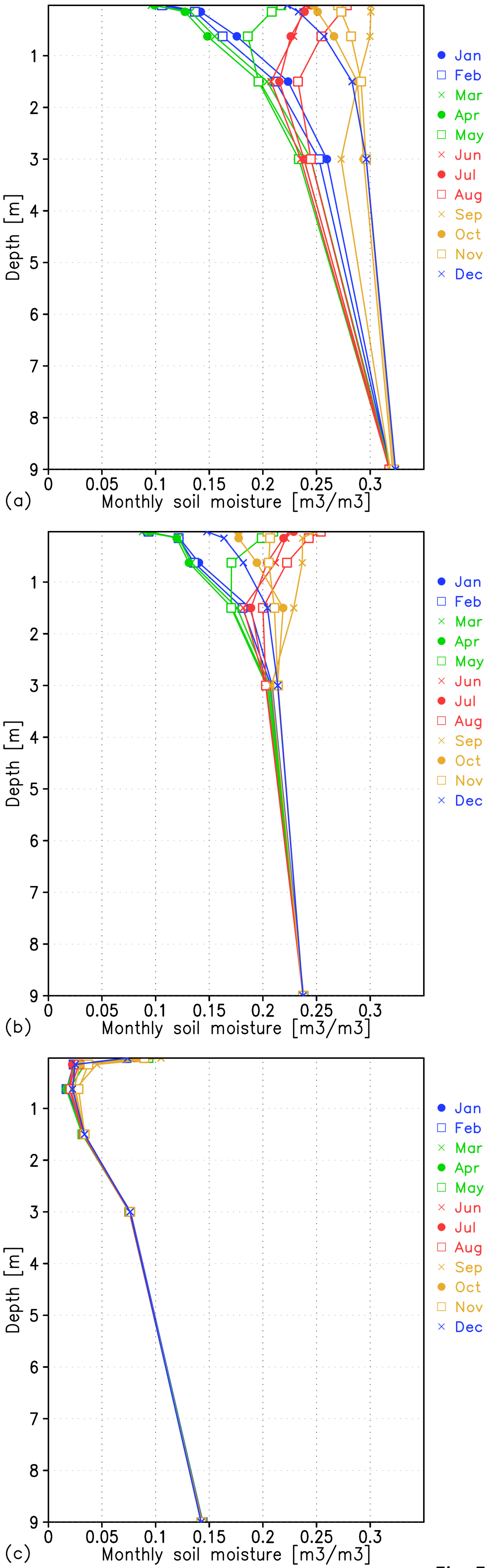
Depth [m]
Monthly soil moisture [m3/m3]
(a)
(b)
(c)
Jan
Feb
Mar
Apr
May
Jun
Jul
Aug
Sep
Oct
Nov
Dec
0
0.05
0.1
0.15
0.2
0.25
0.3
1
2
3
4
5
6
7
8
9

Fig. 5

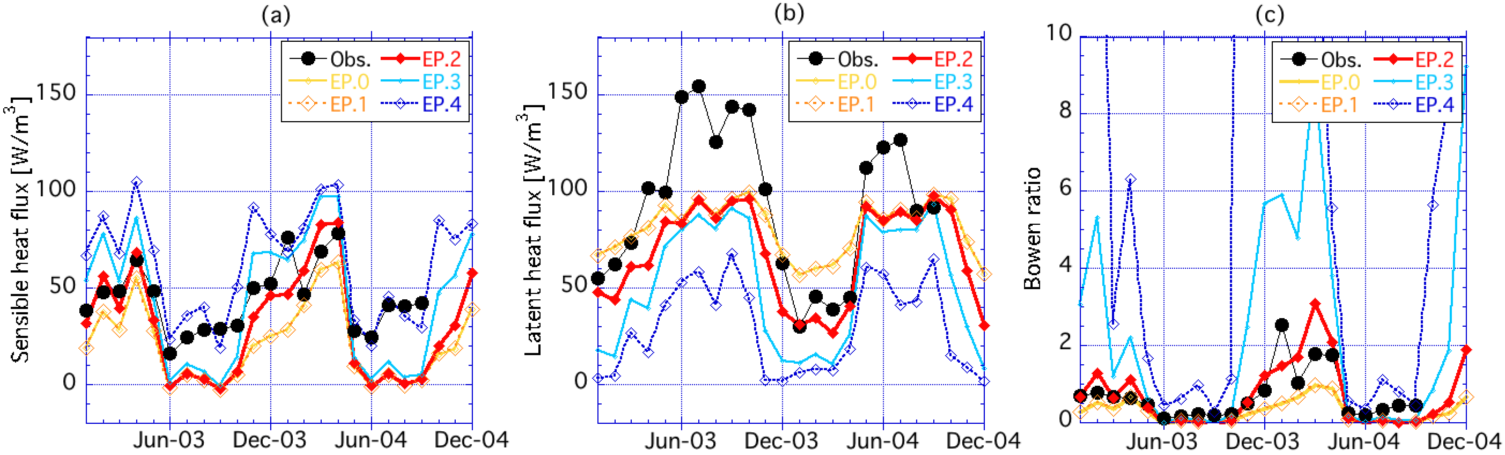
(a)
Sensible heat flux [W/m^3]
Obs.
EP.0
EP.1
EP.2
EP.3
EP.4
150
100
50
0
Jun-03
Dec-03
Jun-04
Dec-04
(b)
Latent heat flux [W/m^3]
(c)
Bowen ratio
10
8
6
4
2

Fig. 6

Fig. 7

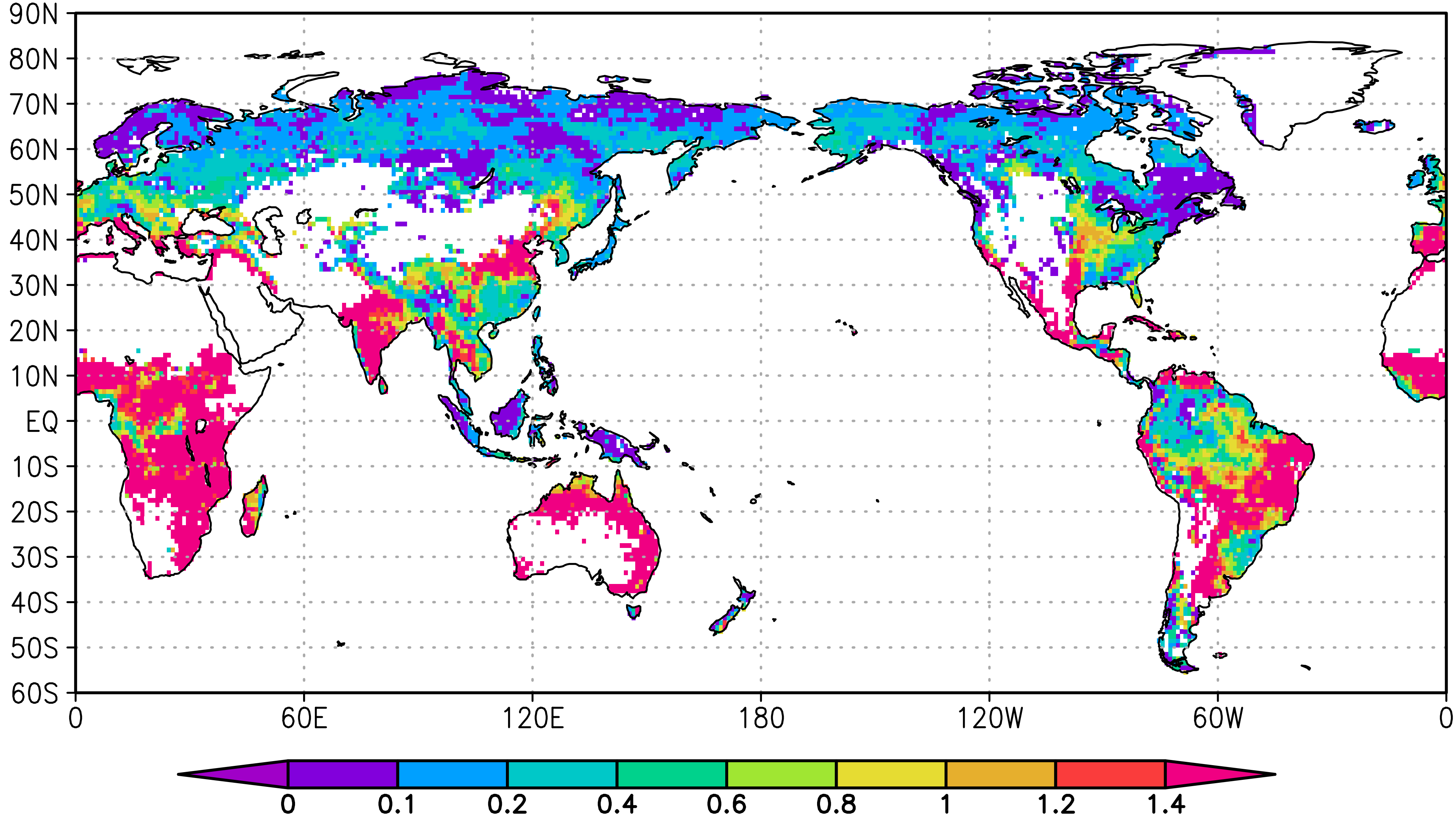
90N
80N
70N
60N
50N
40N
30N
20N
10N
EQ
10S
20S
30S
40S
50S
60S
0
60E
120E
180
120W
60W
0
0
0.1
0.2
0.4
0.6
0.8
1
1.2
1.4

Table 1 List of experiments.

Experiment	ε_{GW}	θ_s–ε_{GW}
EP.0	0.001	~0.4
EP.1	0.1	~0.3
EP.2	0.2	~0.2
EP.3	0.3	~0.1
EP.4	0.4	~0.0

Table 2 Nash–Sutcliffe efficiency of modeled daily river flow compared to observed river flow at the inlet of the Bhumibol dam in 2002 (rainy year) and 1993 (dry year).

Experiment	2002	1993
EP.0	–0.357	–0.376
EP.1	–0.258	–0.358
EP.2	0.250	0.763
EP.3	–1.706	–11.28
EP.4	–5.197	–46.77